

# Preferential Adsorption of TiO<sub>2</sub> Nanostructures on Functionalized Single-Walled Carbon Nanotubes: A DFT Study

Serge Ayissi,<sup>†</sup> Paul A. Charpentier,<sup>\*,†</sup> Krisztián Palotás,<sup>‡</sup> Nasrin Farhangi,<sup>†</sup> Felix Schwarz,<sup>§</sup> and Werner A. Hofer<sup>||</sup>

<sup>†</sup>Department of Chemical and Biochemical Engineering, University of Western Ontario, London, Ontario N6A 5B9, Canada

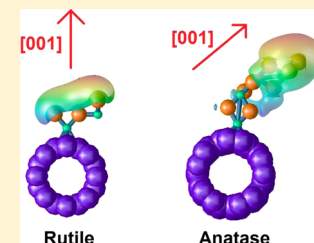
<sup>‡</sup>Department of Theoretical Physics, Budapest University of Technology and Economics, Budapest, Hungary

<sup>§</sup>Surface Science Research Centre, University of Liverpool, Liverpool L69 3BX, United Kingdom

<sup>||</sup>Faculty of Science, Agriculture and Engineering, Newcastle University, Newcastle upon Tyne NE1 7RU, United Kingdom

## Supporting Information

**ABSTRACT:** The mechanism of attachment of nanocrystals (NCs) to curved carbonaceous species such as graphene nanoribbons and carbon nanotubes (CNTs) is of current scientific interest. In addition, we have observed anisotropic growth patterns of titania NCs from carbonaceous materials, for which there is no theoretical explanation. In this work, we use density functional theory (DFT) calculations for calculating the energy of adsorption of titania nanostructures to both armchair metallic and zigzag semiconducting single-walled carbon nanotubes (SWCNTs) in their pure and functionalized forms. Several adsorption sites are considered including top, bridge, and hollow sites for pure SWCNTs, while for functionalized SWCNTs epoxy, alcohol, and carboxylate are examined. Results from binding energy calculations were found to predict favorable adsorption of TiO<sub>2</sub> NCs on the chemical adsorption sites of functionalized SWCNTs compared to the physical adsorption sites of pure SWCNTs. The rotation of anatase and rutile titania species on the physical adsorption sites showed interesting behavior particularly regarding binding strength and growth direction predictions. Partial density of states (PDOS) calculations examined the electronic structure of the assemblies. Charge density maps showed the importance of chemisorption sites for interactions between titania structures and SWCNTs. Electronic local potentials showed the difference in binding strengths for anatase titania on SWCNT physical adsorption sites. These results provide new theoretical evidence for controlled and oriented growth mechanisms on curved carbon-based substrates that have applications in various emerging applications from photovoltaic devices to nanomedicine.



## INTRODUCTION

Since their discovery by Iijima in 1991,<sup>1</sup> single walled carbon nanotubes (SWCNTs) have been suggested as candidate materials for numerous applications including nanoelectronic devices, fuel cells, photovoltaic devices, and delivery vehicles for nanomedicines. Their unique carbon sp<sup>2</sup> structure provides exceptional physical, chemical, and electrical properties including thermal conductivity,<sup>2</sup> electrical mobility, and mechanical stability.<sup>3–5</sup> The wide range of applications for SWCNTs has led to the development of a large number of synthetic techniques for their preparation.<sup>6</sup> However, these growth techniques are not selective enough to control the nanotube's diameter or chirality,<sup>7–11</sup> which are known to control their electronic behavior.<sup>3</sup> For the SWCNT, either the metallic or semiconducting property dominates the components that will affect the charge separation efficiency. Due to effective charge separation across the semiconducting TiO<sub>2</sub>/SWCNT interface,<sup>12</sup> semiconducting CNTs are better than metallic CNTs as photosensitizers to enhance photoactivity. The semiconducting TiO<sub>2</sub>/CNT interface can potentially form an excellent photovoltaic solar cell if the charge transfer can be increased. In contrast, the metallic TiO<sub>2</sub>/CNT interface provides significant charge transfer, resulting in a small built-

in potential. What can control this charge transfer is unknown, although nanocrystals of semiconducting particles interacting with SWCNTs can potentially improve the charge separation.<sup>13,14</sup>

Of the well-known semiconductors, titanium dioxide (TiO<sub>2</sub>) has been investigated for a variety of applications, including environmental remediation<sup>15</sup> and solar materials such as dye-sensitized solar cells (DSSCs).<sup>16,17</sup> The two main crystalline structures of TiO<sub>2</sub> are anatase and rutile.<sup>18</sup> Tetragonal rutile structure belongs to the P4<sub>2</sub>/mnm ( $D_{4h}^{14}$ ) space group containing 6 atoms per primitive cell as Ti<sub>2</sub>O<sub>4</sub>. Tetragonal anatase structure belongs to the I4<sub>1</sub>/amd ( $D_{4h}^{19}$ ) space group containing 12 atoms per primitive cell as Ti<sub>4</sub>O<sub>8</sub>.

Anatase TiO<sub>2</sub> is a metastable crystal state that has been extensively investigated due to its well-known photocatalytic activity while also having a lower electron–hole recombination rate. Rutile is a thermodynamically stable phase possessing a smaller band gap energy<sup>19</sup> (3.0 eV) compared to anatase<sup>20</sup> (3.2 eV), giving lower photoactivity. A large amount of research has

Received: February 10, 2015

Revised: June 12, 2015

Published: June 14, 2015

aimed to modify the properties of  $\text{TiO}_2$ , specifically to decrease the electron–hole recombination rate<sup>18</sup> while extending its light absorption into the visible region. Previously, we examined the synthesis of titania–graphene composites<sup>21</sup> and iron-doped titania nanoassemblies in the green solvent, supercritical  $\text{CO}_2$ ,<sup>22</sup> as well as their resulting properties, which improved significantly compared to bare titania. Our group has also carried out DFT simulations on the behavior of titania in  $\text{CO}_2$ , demonstrating  $\text{CO}_2$ -philicity arising from the metal acetate groups,<sup>23,24</sup> illustrating the importance of theoretical calculations for understanding the physical and chemical mechanisms operating in these systems.

To date, a detailed theoretical understanding of the chemical and physical interactions between  $\text{TiO}_2$  nanostructures and SWCNTs as well as their charge transfer mechanism is unknown. DFT calculations,<sup>12</sup> studying the photovoltaic properties of interfaces of bulk titanium with mixed semiconducting and metallic CNTs, have shown that  $\text{TiO}_2/\text{CNT}$  interfaces can be useful as photovoltaic materials if they are decorated by a metal cluster. However, the details on the chemical and electronic interactions between nanostructured  $\text{TiO}_2$  and pure or functionalized CNTs have not been investigated theoretically. In the present study, we investigated the interaction of  $\text{TiO}_2$  and CNTs through two possible adsorption mechanisms: physisorption and chemisorption along with detailed charge transfer calculations.

## COMPUTATIONAL DETAILS

Electronic structure calculations were carried out using the GGA PW91<sup>25</sup> functional implemented in VASP code<sup>26,27</sup> for all CNT and titania systems. The GGA PW91 functional previously provided a higher efficiency for stabilizing the anionic adsorption of carbon-based compounds to  $\text{TiO}_2$  surfaces.<sup>28</sup> The electron–ion interaction is described by the projector-augmented wave (PAW) scheme,<sup>29,30</sup> the electronic wave functions were expanded using plane waves with a kinetic energy up to 400 eV, and the  $k$ -point sampling was set to  $3 \times 2 \times 1$  for the geometry optimization of periodic systems specifically and to  $5 \times 5 \times 1$  for the electronic structure. The Brillouin zone was described using a Monkhorst–Pack<sup>31</sup> (M&P) scheme of special  $k$ -points. Convergence criteria of  $5 \times 10^{-3}$  eV for energies and 0.01 eV/Å for forces acting on ions in structural optimizations were used. Band diagrams and density of states (DOS) analysis were obtained by fixing the Wigner–Seitz radius ( $rw_{\text{igs}}$ ) for the support during integration over the number of electrons and then by setting  $rw_{\text{igs}}$  for the adsorbates within the radii of tangential spheres. This method allowed the accurate assignment of relevant atomic orbital attributions to a particular projected DOS peak. All systems were modeled using the supercell approach with periodically repeated slabs. Models of pure and functionalized armchair and zigzag CNT substrates were used. Six adsorption sites were considered: top, bridge, and hollow sites on the pure CNT and CNT-ol, carboxylate, and epoxy sites on the functionalized CNT. Parts a–c of Figure 1 show the schematic structures of titania species adsorbed on all possible sites of a pure CNT, while parts d–f of Figure 1 show the potential adsorption sites for titania species on functionalized CNTs.

Single walled carbon nanotubes (SWCNTs) were constructed by rolling up graphene to form a cylinder. The circumference of the SWCNT is determined by the two primitive vectors  $\vec{a}_1$  and  $\vec{a}_2$ , the chiral vector  $C_h = n\vec{a}_1 + m\vec{a}_2$ ,

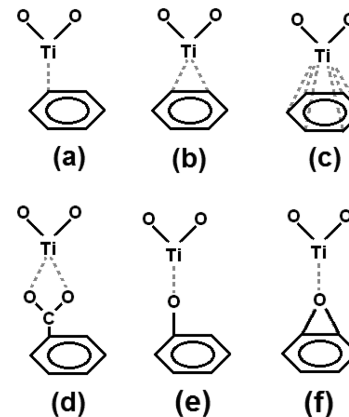


**Figure 1.** Adsorption sites of clean CNT and functionalized CNTs.  $\text{TiO}_2$  adsorbates can be located at (a) top, (b) bridge, and (c) hollow sites of CNT.  $\text{TiO}_2$  can also be located at (d) carboxylate, (e) CNT-ol, and (f) epoxy sites of functionalized CNTs.

and the lattice parameter of the graphene honeycomb structure  $a_0$ . The primitive vectors of graphene are the following

$$\vec{a}_1 = a_0 \sqrt{3} \left( \frac{1}{2}, \frac{\sqrt{3}}{2} \right), \quad \vec{a}_2 = a_0 \sqrt{3} \left( -\frac{1}{2}, \frac{\sqrt{3}}{2} \right) \quad (1)$$

where  $a_0 = 1.42$  Å is the C–C bond length. The 2D graphene sheet together with the  $\vec{a}_1$ ,  $\vec{a}_2$ , and  $C_h$  vectors specifying the chirality of the nanotube are as shown in Figure 2. A lattice point O is chosen as the origin.

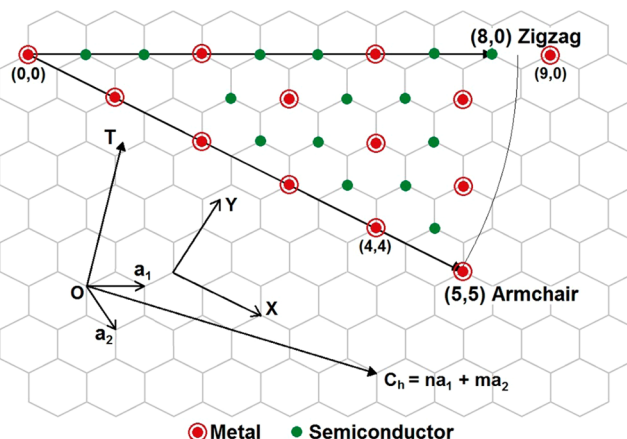


**Figure 2.** 2D graphene sheet shown with integers  $(n, m)$  specifying chiral vectors  $C_h$  for carbon nanotubes, including zigzag if  $n$  or  $m$  equals zero or armchair if  $n = m$ . The red circled dots denote metallic tubules, while the small green dots are for semiconducting tubules.<sup>3,32</sup>

Figure 2 also shows the physical properties of the carbon nanotubes formed with respect to the pair of integers  $(n, m)$ .<sup>3,32</sup>

Both metallic and semiconducting SWCNTs can be formed from armchair, zigzag, and chiral tubules.<sup>33</sup> The diameter of a (5,5) armchair SWCNT is expected to be slightly longer than the diameter of a (8,0) zigzag SWCNT, respectively 6.78 and 6.27 Å theoretically. A (9,0) zigzag SWCNT is closer in diameter, 7.05 Å, to a (5,5) armchair SWCNT but has similar physical properties, as it is also metallic. A semiconducting (8,0) zigzag SWCNT is preferred as opposed to the metallic properties of the (5,5) armchair SWCNT.<sup>3,32</sup>

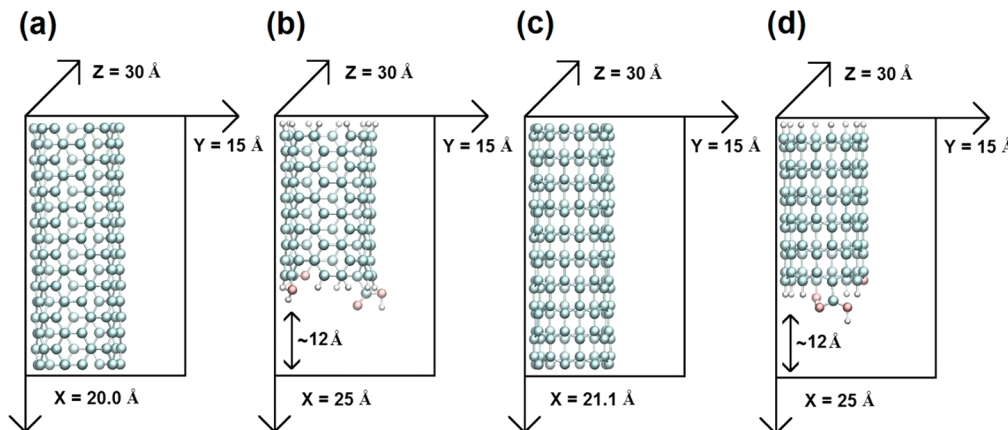


**Figure 3.** Optimized structures of (a) a (5,5) armchair SWCNT, (b) a (5,5) functionalized armchair SWCNT, (c) a (8,0) zigzag SWCNT, and (d) a (8,0) functionalized zigzag SWCNT.

Chemical functionalization is known experimentally to occur preferentially at the edges of SWCNTs.<sup>7,8,10,11</sup> As the limitations of DFT calculations allow only small system sizes, functionalized CNTs were used separately from pure SWCNTs to study the adsorption on newly formed adsorption sites due to functionalization. The supercells for pure and functionalized CNTs are shown in Figure 3, which contain 160 carbon atoms. Pure armchair and zigzag CNTs were fully optimized in rectangular simulation boxes of respectively 20.0 Å × 15.0 Å × 30.0 Å and 21.1 Å × 15.0 Å × 30.0 Å, as shown on Figure 3a and c. The finite and functionalized armchair and zigzag SWCNTs were also fully optimized in rectangular simulation boxes of 25.0 Å × 15.0 Å × 30.0 Å, as shown in Figure 3b and d. Spin polarization was considered in all calculations, and the electronic structures were optimized to their ground states.

Figure 4a and b show two of the most stable titania surfaces, namely, the (100) and (001) for rutile and the (010) and (100) for anatase.<sup>13,14</sup> To provide an accurate description of a site by site adsorption to SWCNTs, smaller models of titania were considered. Rigid structures were set up for both rutile and anatase due to the previously reported metastability of small size titania nanostructures of bulk properties.<sup>34</sup> Models of a TiO<sub>2</sub> molecule converged in a vacuum, a rutile nanostructure (Ti<sub>2</sub>O<sub>4</sub>), and an anatase nanostructure (Ti<sub>4</sub>O<sub>8</sub>) were used both containing the smallest stoichiometric ratios that provided accurate structure yet facilitated computational convergence.<sup>6,35</sup> The anatase unit cell has a more compact structure than rutile, as the bond distances and angles are slightly smaller.<sup>6,21</sup> Figure 4 also shows the schematic structures of the titania slabs containing stoichiometric models for site by site adsorption.

The isolated TiO<sub>2</sub> molecule was calculated in a large rectangular supercell (10.0 × 10.0 × 20.0 Å) and structurally optimized. The rutile TiO<sub>2</sub> unit cell (Ti<sub>2</sub>O<sub>4</sub>) was initially calculated in a small rectangular supercell (4.6 × 4.6 × 2.9 Å) for a structural optimization of bulk properties. Then, the isolated rutile had its wave function optimized in a large rectangular supercell (10.0 × 10.0 × 20.0 Å). The anatase TiO<sub>2</sub> unit cell (Ti<sub>4</sub>O<sub>8</sub>) was initially calculated in a small rectangular supercell (3.7 × 3.7 × 9.5 Å) also for a geometry optimization in bulk. After that, anatase had its wave function optimized in a large rectangular supercell (10.0 × 10.0 × 20.0 Å). Spin polarization was considered in all calculations, and the electronic structures were optimized to their ground state.

The adsorption energy ( $E_{\text{ads}}$ ) is calculated according to

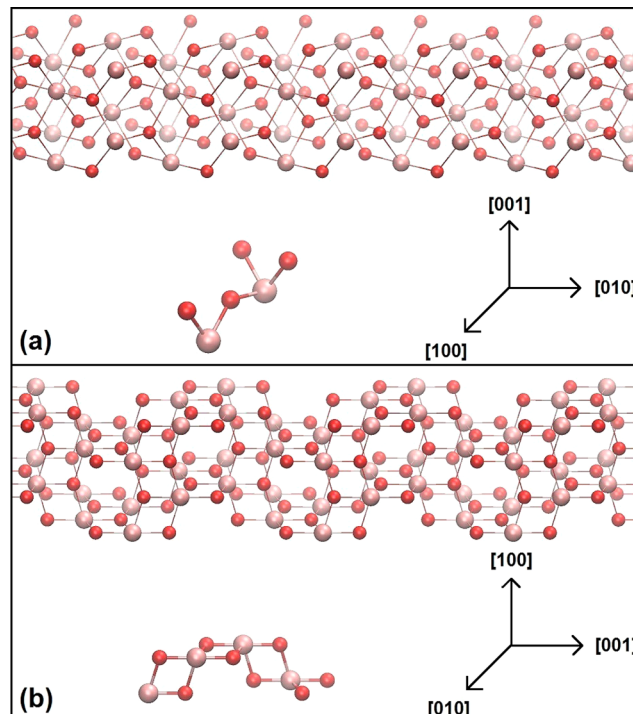


**Figure 4.** Optimized structures of (a) bulk rutile titania with the highlighted Ti<sub>2</sub>O<sub>4</sub> structural unit cell and (b) bulk anatase titania with the highlighted Ti<sub>4</sub>O<sub>8</sub> structural unit cell. Pink and red spheres respectively represent titanium and oxygen.<sup>35</sup>

$$E_{\text{ads}} = E_{(\text{TiO}_2/\text{CNT})} - (E_{\text{TiO}_2} + E_{\text{CNT}}) \quad (2)$$

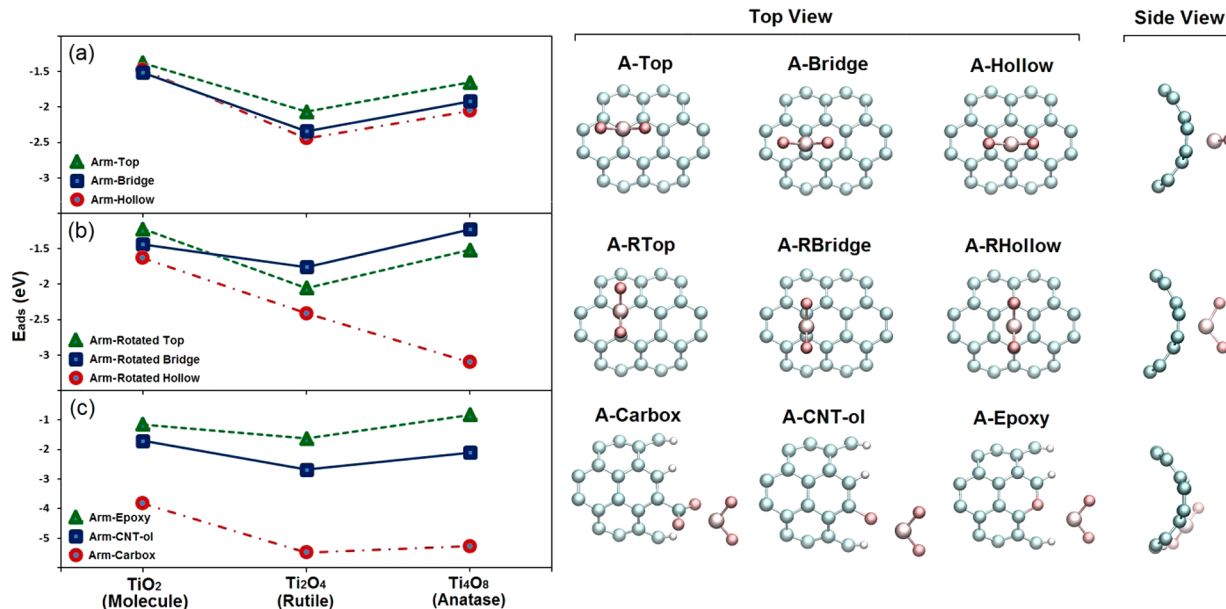
where  $E(\text{CNT})$ ,  $E(\text{TiO}_2)$ , and  $E(\text{TiO}_2/\text{CNT})$  denote, respectively, the calculated energy of a pure CNT, the isolated titanium oxide molecule or nanostructure in a vacuum, and the total energy of a TiO<sub>2</sub>/CNT unit cell adsorbed to the CNT. A negative value of  $E_{\text{ads}}$  implies that the adsorption of the crystalline TiO<sub>2</sub> adsorbate is thermodynamically stable on its CNT substrate.

## RESULTS AND DISCUSSION

**Interaction of TiO<sub>2</sub> Species with Functionalized Armchair (5,5) SWCNTs.** Armchair SWCNTs have three main physical adsorption sites on their outside wall,<sup>36</sup> which are the top, bridge, and hollow sites, as described in Figure 1.

**Table 1.** Adsorption Energies ( $E_{\text{ads}}$ ) and Interaction Distances ( $D_{\text{ads}}$ ) for  $\text{TiO}_2$  Species Adsorbed on Armchair CNTs

site/(interaction type)	molecular $\text{TiO}_2$		rutile or $\text{Ti}_2\text{O}_4$		anatase or $\text{Ti}_4\text{O}_8$	
	$E_{\text{ads}}$ (eV)	$D_{\text{ads}}$ (Å)	$E_{\text{ads}}$ (eV)	$D_{\text{ads}}$ (Å)	$E_{\text{ads}}$ (eV)	$D_{\text{ads}}$ (Å)
top/(Ti–C)	−1.38	2.55	−2.07	2.21	−1.65	2.13
bridge/(Ti–C)	−1.51	2.58	−2.34	2.28	−1.92	2.13
hollow/(Ti–C)	−1.48	2.74	−2.44	2.47	−2.05	2.40
rotated top/(Ti–C)	−1.22	2.52	−2.05	2.21	−1.52	2.15
rotated bridge/(Ti–C)	−1.44	2.56	−1.76	2.27	−1.23	2.32
rotated hollow/(Ti–C)	−1.63	2.72	−2.41	2.45	−3.10	2.37
epoxy/(Ti–O)	−1.20	2.25	−1.83	2.03	−1.94	2.05
carboxylate/(Ti–O)	−3.63	2.12	−5.79	2.03	−5.41	1.95
CNT-ol/(Ti–O)	−2.19	1.99	−3.61	1.90	−3.11	1.89

**Figure 5.** Adsorption energies of  $\text{TiO}_2$  species on armchair functionalized CNTs. (a) Adsorption energy per titania species adsorbed on top, bridge, and hollow. (b) Adsorption energy per titania species adsorbed on rotated top, rotated bridge, and rotated hollow. (c) Adsorption energy per titania species adsorbed on carboxylate, CNT-ol, and epoxy.

Functionalized armchair SWCNTs can have additional adsorption sites, epoxy, CNT-ol, and carboxylate, due to functional groups that are introduced onto their surface during synthesis, which are concentrated at the edges. Functionalized SWCNT edges have been reported as favoring electron transport while binding to flat titania surfaces.<sup>37,38</sup> The interaction between titania species and armchair (5,5) SWCNTs was studied on all physical and chemical adsorption sites summarized in Table 1. The physical adsorption sites depend on the geometry of the adsorbate and direction of adsorption. Rotating the adsorbate by 90° created the “rotated” version of a physical adsorption site.

Figure 5a shows a comparison of the adsorption strength of the three studied species: molecular  $\text{TiO}_2$ , rutile ( $\text{Ti}_2\text{O}_4$ ), and anatase ( $\text{Ti}_4\text{O}_8$ ) adsorbed at similar adsorption sites that are the top, the bridge, and the hollow site of pure CNT. Figure 5b shows the identical adsorption sites of CNT, with the titania adsorbates rotated by 90°; these adsorption sites are termed rotated top, rotated bridge, and rotated hollow. Finally, Figure 5c shows all the Ti–O interactions between the titania species and the organic adsorption sites that are carboxylate, CNT-ol, and epoxy.

Molecular  $\text{TiO}_2$  was found to physisorb preferentially on a bridge site, followed by the hollow site and then the top site of

armchair SWCNTs. The rotated hollow site was found to be the most favorable, slightly above 1.6 eV, followed by the rotated bridge and the rotated top of an adsorbed rotated molecular  $\text{TiO}_2$  on CNT. Molecular  $\text{TiO}_2$  was found to bind the closest to armchair SWCNT on the top and rotated top sites at 2.55 and 2.52 Å, respectively. The binding energy and distances correspond to a Ti–C noncovalently bonded interaction<sup>39,40</sup> in the physical adsorption process. The  $\text{TiO}_2$  molecule was found to chemisorb preferentially on the edge-located carboxylate site, slightly above 3.6 eV, followed by the edge located CNT-ol site.  $\text{TiO}_2$  adsorbs to the CNT-ol site closest at a Ti–O noncovalently bonded distance of 1.99 Å. The epoxy adsorption site of the CNTs was found to have the weakest binding energy of the Ti–O nonbonded interactions attributed to the fact that titania physisorbs to epoxy while it chemisorbs to carboxylate and CNT-ol.

Rutile ( $\text{Ti}_2\text{O}_4$ ) was found to adsorb preferentially on a hollow site, followed by the bridge site and then the top site of armchair SWCNT. The rotated hollow site was found to be the most favorable, slightly above 2.4 eV, followed by the rotated top and then the rotated bridge of an adsorbed rotated rutile ( $\text{Ti}_2\text{O}_4$ ) on armchair CNT. Rutile binds the closest to armchair SWCNT on the top and rotated top sites at 2.21 Å. Rutile ( $\text{Ti}_2\text{O}_4$ ) adsorbs preferentially on the edge located carboxylate

Table 2. Adsorption Energies ( $E_{\text{ads}}$ ) and Interaction Distances ( $D_{\text{ads}}$ ) for  $\text{TiO}_2$  Species Adsorbed on Zigzag CNTs

site/(interaction type)	molecular $\text{TiO}_2$		rutile or $\text{Ti}_2\text{O}_4$		anatase or $\text{Ti}_4\text{O}_8$	
	$E_{\text{ads}}$ (eV)	$D_{\text{ads}}$ (Å)	$E_{\text{ads}}$ (eV)	$D_{\text{ads}}$ (Å)	$E_{\text{ads}}$ (eV)	$D_{\text{ads}}$ (Å)
top/(Ti–C)	-1.45	2.46	-2.33	2.25	-1.90	2.13
bridge/(Ti–C)	-1.57	2.50	-2.41	2.34	-2.12	2.12
hollow/(Ti–C)	-1.52	2.84	-2.86	2.47	-3.11	2.40
rotated top/(Ti–C)	-1.42	2.48	-2.44	2.25	-2.04	2.15
rotated bridge/(Ti–C)	-1.53	2.52	-2.39	2.37	-1.94	2.30
rotated hollow/(Ti–C)	-1.40	2.84	-2.71	2.53	-2.56	2.41
epoxy/(Ti–O)	-1.15	2.20	-1.63	2.10	-0.83	2.11
carboxylate/(Ti–O)	-3.83	2.10	-5.48	2.00	-5.27	1.97
CNT-ol/(Ti–O)	-1.71	2.04	-2.68	1.92	-2.11	1.89

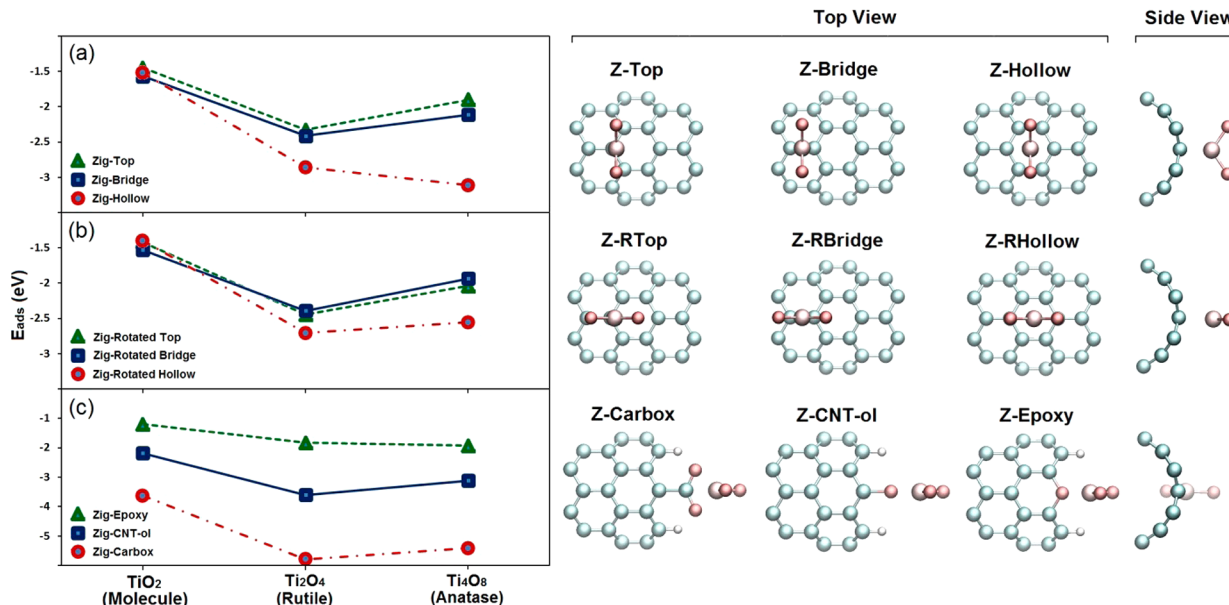


**Figure 6.** Adsorption energies of  $\text{TiO}_2$  species on zigzag functionalized CNTs. (a) Adsorption energy per titania species adsorbed on top, bridge, and hollow. (b) Adsorption energy per titania species adsorbed on rotated top, rotated bridge, and rotated hollow. (c) Adsorption energy per titania species adsorbed on carboxylate, CNT-ol, and epoxy.

site followed by the edge located CNT-ol site. The carboxylate site adsorbs rutile ( $\text{Ti}_2\text{O}_4$ ) the strongest, around 5.8 eV, but this adsorption site can only be found on the edges of the CNT. The epoxy adsorption site of the CNTs was found to have the weakest binding energy of the Ti–O nonbonded interactions, slightly above 1.8 eV.

The rotated hollow was found to be the site onto which anatase ( $\text{Ti}_4\text{O}_8$ ) adsorbs the strongest on armchair SWCNTs; the binding energy here is slightly above 3.1 eV. Anatase physisorbs preferentially to rotated hollow and hollow sites followed by the other physical adsorption sites including the epoxy. Anatase ( $\text{Ti}_4\text{O}_8$ ) was found to chemisorb preferentially on the edge located carboxylate site followed by the edge located CNT-ol site of the functionalized armchair SWCNT. The carboxylate site adsorbs anatase ( $\text{Ti}_4\text{O}_8$ ) the strongest, above 5.4 eV, but this adsorption site can only be found on the edges of the CNT. The epoxy adsorption site of the CNTs was found to have the weakest binding energy of the Ti–O nonbonded interactions around 1.9 eV.

**Interaction of  $\text{TiO}_2$  Species with Functionalized Zigzag (8,0) SWCNTs.** Zigzag SWCNTs also have three main physical adsorption sites on their outside wall,<sup>36</sup> which are the top, bridge, and hollow sites and additional adsorption sites, epoxy, CNT-ol, and carboxylate, due to functionalization. The

interactions between titania species and zigzag (8,0) SWCNTs were studied on all physical and chemical adsorption sites. The results of DFT calculated noncovalently<sup>39,40</sup> bonded Ti–C and Ti–O binding energies and distances between titania and zigzag SWCNT are shown in Table 2.

Figure 6a shows a comparison of adsorption strengths of the three studied species, the molecular  $\text{TiO}_2$ , the rutile ( $\text{Ti}_2\text{O}_4$ ), and the anatase ( $\text{Ti}_4\text{O}_8$ ), adsorbed at similar adsorption sites that are the top, the bridge, and the hollow site of pure CNTs. Figure 6b shows the identical adsorption sites of CNT, with the similar titania adsorbates which were rotated by 90°. Finally, Figure 6c shows all the Ti–O interactions between the titania species and the organic adsorption sites that are carboxylate, CNT-ol, and epoxy.

A similar trend in Ti–C interactions can be observed, while the titania species adsorb on zigzag SWCNTs compared to adsorption on armchair SWCNTs. Some differences on physical adsorption sites can still be observed. For molecular  $\text{TiO}_2$ , the bridge site was found to be the most favorable energetically, slightly below 1.57 eV. Rutile ( $\text{Ti}_2\text{O}_4$ ) was found to show a higher binding strength on the hollow site, slightly above 2.8 eV, while anatase ( $\text{Ti}_4\text{O}_8$ ) showed the highest overall physical adsorption energy on the hollow site, slightly above 3.1 eV. For all titania species, the Ti–O interaction adsorption sites

showed similar trends, as carboxylate remains the strongest, followed by the CNT-ol and then the epoxy site.

**Analysis of the Interaction between  $\text{TiO}_2$  and SWCNTs.** The binding energy values of the  $\text{TiO}_2$  species adsorbed on SWCNTs, reported in Tables 1 and 2, show a quantitative difference between solid state  $\text{TiO}_2$  and gas phase  $\text{TiO}_2$  on all adsorption sites. When adsorbed on CNTs, solid state  $\text{TiO}_2$  is thermodynamically more stable than gas phase  $\text{TiO}_2$  due to a lower entropy of adsorption.<sup>41</sup> As a result, binding distances of structural  $\text{TiO}_2$  are shorter than molecular  $\text{TiO}_2$  for similar reasons. The calculated strength and distances of adsorption on functionalized SWCNT sites confirm this tendency. Rutile  $\text{TiO}_2$  generally binds stronger while anatase binds closer to SWCNTs. Both rutile and anatase bind stronger and closer to SWCNTs than molecular  $\text{TiO}_2$ . There are two adsorption sites on armchair and zigzag SWCNTs that show a higher binding strength for anatase  $\text{TiO}_2$  with respect to rutile. These sites are the rotated hollow site of armchair (5,5) SWCNT and the hollow site of zigzag (8,0) SWCNT.

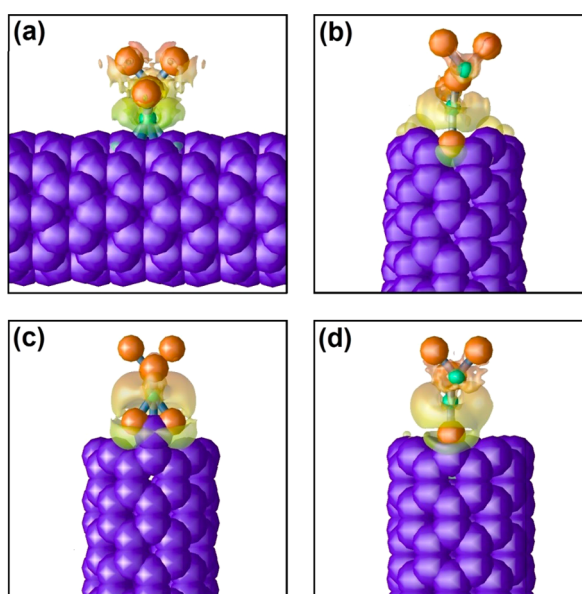
Further understanding on the difference of binding energies for  $\text{TiO}_2$  species adsorbed to the SWCNTs can be gained by calculating the real space charge redistribution, as the binding energy may have electrostatic origins.

Figure 7a–d show the electrostatic density map at the binding region of  $\text{Ti}_2\text{O}_4$  adsorbed on, respectively, hollow,

physisorbs to both hollow and epoxy sites. The proximity of rutile to the six carbons of the SWCNT hollow site creates an additional binding strength helping to explain the difference between the adsorption on hollow with the adsorption on other physical adsorption sites.<sup>21</sup> The density contour maps shown in Figure 7c and d indicate that a much larger electrostatic interaction exists between the substrate terminated by ( $\text{COO}^-$ ) and also ( $\text{O}^-$ ), and the titania. This is attributed to the fact that in these cases titania chemisorbs to carboxylate and CNT-ol. A clear concentration of charge renders a continuous electron density along the  $z$  axis. The electrostatic density of titania–( $\text{COO}^-$ ) and titania–( $\text{O}^-$ ) binding regions confirms the presence of a maximum force of attraction due to the ionic nature of carboxylate and CNT-ol adsorption sites. For the carboxylate group, the charge density is increasingly accumulated along the nonbonded interaction axis of the  $\text{TiO}_2$ –CNT binding region due to the presence of the two oxygen atoms. These maps confirm the importance of the electron distribution property in the interaction between titania and SWCNTs.

Although the electronic structures of rutile and anatase  $\text{TiO}_2$  were previously investigated<sup>18,42</sup> along with CNTs<sup>5,43</sup> and functionalized CNTs,<sup>7–11,44</sup> the electronic structure of  $\text{TiO}_2$  on CNT has only been considered for larger diameter CNTs having interfacial interactions with bulk  $\text{TiO}_2$ .<sup>12</sup> Hence, we investigated the partial density of states (PDOS) of anatase  $\text{TiO}_2$  nanostructures adsorbed on armchair SWCNTs at the calculated most stable adsorption sites, i.e., the hollow site and the rotated hollow site. After the binding energetics and structural morphologies of  $\text{TiO}_2$  clusters adsorbed on SWCNTs and functionalized SWCNTs were investigated, the electronic structures of all systems were studied in order to determine the relation between PDOS and the binding energy. As the difference between rutile and anatase titania has already been studied by PDOS,<sup>18,42</sup> we focused our study on the difference in binding strength for anatase  $\text{TiO}_2$  adsorbed on hollow and rotated hollow sites of armchair and zigzag SWCNTs. As previously mentioned, rotating the anatase  $\text{TiO}_2$  nanostructures adsorbed on CNTs by  $90^\circ$  from hollow to rotated hollow increases the binding energy by more than 1.1 eV for the armchair CNTs (see Table 1) and decreases the binding energy by 0.6 eV for the zigzag CNTs. The PDOS for the C 2p band of CNT and the O 2p and Ti 3d bands of anatase  $\text{TiO}_2$  adsorbed on a hollow site and a rotated hollow site of armchair SWCNT are displayed, respectively, in Figure 8a and b. To facilitate an understanding of how O 2p, Ti 3d, and C 2p states are modified upon adsorption, the C 2p band of armchair SWCNT was isolated from that of  $\text{TiO}_2$  after adsorption of nanostructural  $\text{TiO}_2$ .

While adsorbed on hollow and rotated hollow sites of armchair SWCNTs, the PDOS of O and Ti atoms of anatase titania display clear semiconducting properties. Their valence and conduction bands are spaced around the Fermi level ( $E_F$ ) referenced at 0 eV. The valence band is dominated by O 2p orbitals with a small contribution from the Ti 3d orbitals, whereas Ti 3d dominates the conduction band with a small contribution from O 2p. The intrinsic band gaps of  $\text{TiO}_2$  nanostructures have no changes, implying that the electron transition from the O 2p at the valence band and the Ti 3d at the conduction band is not the dominant process in the interactions between anatase  $\text{TiO}_2$  and armchair CNT. The lower theoretical value of band gaps with respect to experimental data is caused by a shortage in the DFT



**Figure 7.** Real space view of the charge redistribution  $\Delta Q = Q_{(\text{TiO}_2/\text{CNT})} - (Q_{\text{TiO}_2} + Q_{\text{CNT}})$  for (a)  $\text{Ti}_2\text{O}_4$  physisorbed on a hollow site of pure CNT, (b)  $\text{Ti}_2\text{O}_4$  physisorbed on an epoxy site of functionalized CNT, (c)  $\text{Ti}_2\text{O}_4$  chemisorbed on a carboxylate site of functionalized CNT, and (d)  $\text{Ti}_2\text{O}_4$  chemisorbed on a hydroxylate site of functionalized CNT. The isosurface value is set to  $-20.0$  and the opacity to  $0.50$ .

epoxy, carboxylate, and CNT-ol sites of zigzag SWCNTs. The Ti–C interaction of  $\text{Ti}_2\text{O}_4$  with a hollow site of zigzag CNT is perpendicular to the CNT surface along the tube axis, and the electrostatic Ti–O interaction of  $\text{Ti}_2\text{O}_4$  with epoxy, carboxylate, or CNT-ol is parallel to the CNT surface along the tube axis. Most of the rutile electronic density is created by the presence of oxygen. The density maps in Figure 7a and b show that a clear electrostatic gap exists in the binding region as titania

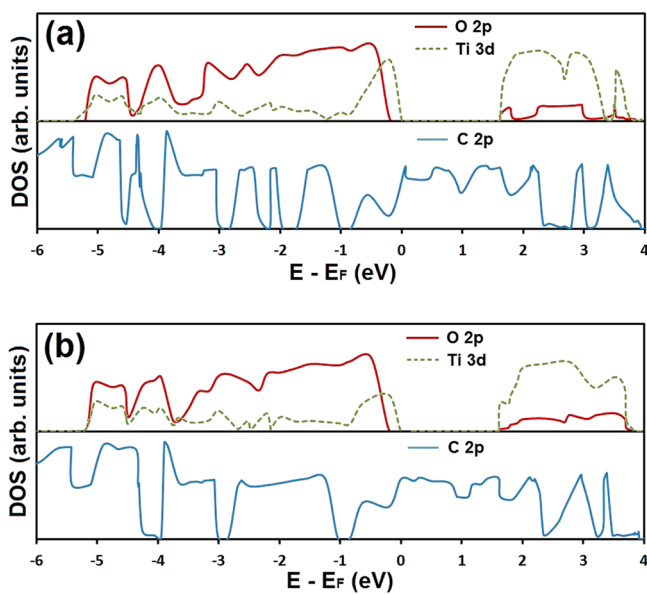


**Figure 8.** Partial density of states (PDOS) for anatase  $\text{TiO}_2$  physisorbed on armchair SWCNT at (a) a hollow site and (b) a rotated hollow site. C 2p curves of both systems have been separated from O 2p and Ti 3d curves for clarity.

estimation, mostly due to the self-correlation error of electrons and to the difference between small clusters and bulk matter.<sup>45,46</sup>

By comparing the C 2p bands of armchair SWCNT in Figure 8a and b, it is immediately apparent that armchair SWCNTs with anatase adsorbed at a hollow site and a rotated hollow site do not alter quantitatively the PDOS of C atoms. The carbon bands of SWCNTs have no forward or backward movement of

their Fermi levels, as the titania adsorbates are nonmetallic and nonionic species. Some additional peaks below and above the Fermi level of the C 2p band with anatase can be seen compared to the C 2p band with anatase adsorbed on the rotated hollow site. We assume these peaks are characteristic of the structural defects of SWCNTs at the adsorption region due to C–C bond deformation.<sup>47,48</sup>

**Preferential Adsorption and Direction of Growth of  $\text{TiO}_2$  on Carbon-Based Curved Substrates.** After having an accurate understanding of the SWCNT curved surface properties and the adsorption of titania species, a window opens to engineer surfaces seeking desired directions of growth.<sup>49</sup> According to the above discussions, anatase nanostructures showed a higher binding strength on rotated adsorption sites with respect to normal adsorption sites if the rotation puts the nanostructure in a normal direction with respect to the SWCNTs. The orientation of rutile nanostructures does not affect the binding strength on armchair and zigzag SWCNTs. Figure 9 shows the electrostatic potential maps calculated at the ground states of titania–SWCNT systems. Figure 9a shows the configuration for which anatase adsorbed on SWCNT is unfavorable, especially if anatase sits on the hollow site. This configuration makes growth on the [001] direction unlikely, even though that direction is one of the most favorable for anatase.<sup>49</sup> Figure 9b shows that anatase can then possibly grow along the [001] direction with a maximal electrostatic potential concentrated toward that direction. Anatase can also possibly grow along the [010] and [0-10] directions. On the contrary, rutile adsorbed on SWCNTs along the direction of the CNTs does not affect the binding strength but it limits the possible direction of growth. Figure 9c shows that rutile can possibly grow along the [001] direction similarly to anatase, causing a maximum of

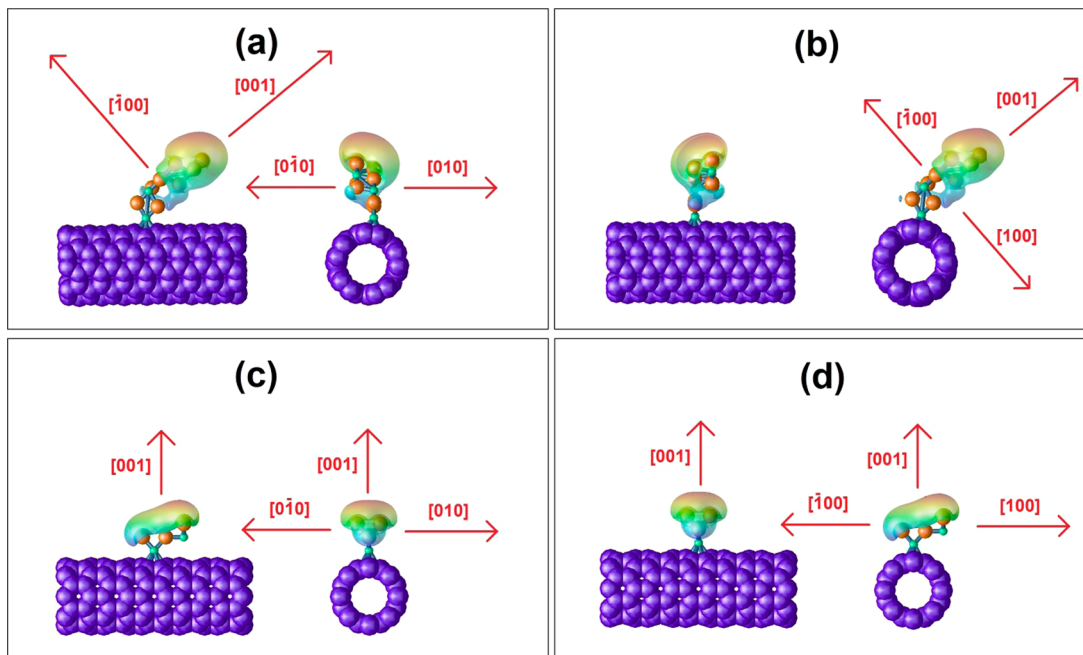


**Figure 9.** Electrostatic potential (EP) maps for anatase and rutile species physisorbed on SWCNT. Anatase sits on (a) the hollow site of armchair SWCNT and (b) the rotated hollow site of armchair SWCNT. Rutile sits on (c) the hollow site of armchair SWCNT and (d) the rotated hollow site of armchair SWCNT. Note that geometrically the hollow site configurations of armchair SWCNT correspond to the rotated hollow site configuration of zigzag SWCNT, while the rotated hollow site configurations correspond to the hollow site configurations. The isosurface value is set to +3.0 and the opacity to 0.50.

electrostatic potential located toward that direction. Rutile can also grow along the [010] and [0-10] similarly to anatase. A 90° rotation of anatase on similar adsorption sites, as shown by Figure 9c, increases the binding strength by 1.05 and 0.55 eV on armchair and zigzag SWCNT, respectively. This is essentially due to the fact that the electrostatic potential located at the edge of the anatase adsorbate points in a normal direction from the nanotubes. The rotation of rutile in Figure 9d does not alter the binding strength with SWCNT but opens a new direction of growth in the [100] and [-100] directions.

## CONCLUSION

We have studied the adsorption of molecular and structural  $\text{TiO}_2$  adsorbates on pure and functionalized (i.e.,  $-\text{COOH}$ ,  $-\text{OH}$ ,  $-\text{O}-$ ) SWCNTs by density functional theory.

We concentrated our investigation on both the metal–carbon ( $\text{Ti}-\text{C}$ ) and metal–oxygen ( $\text{Ti}-\text{O}$ ) interactions with a potential two-dimensional rotation of the adsorbates that leads to new sites, termed “rotated”. The adsorption results show that structural  $\text{TiO}_2$  nanocompounds such as rutile ( $\text{Ti}_2\text{O}_4$ ) and anatase ( $\text{Ti}_4\text{O}_8$ ) have higher binding energies to SWCNTs than those from a simple  $\text{TiO}_2$  molecule.  $\text{Ti}_x\text{O}_{2x}$  ( $x = 2, 4$ ) nanostructures showed higher physical and chemical adsorption on both armchair and zigzag SWCNTs. Anatase nanostructures bind closer to the physical adsorption sites of SWCNTs, while rutile nanostructures bind stronger.

Our charge redistribution maps confirmed the experimentally found evidence that the incorporation of functionalized SWCNTs in the  $\text{TiO}_2$  support provides more efficient electron transfer through the film in dye-sensitized solar cells.<sup>38</sup> The electron transport is in fact facilitated by functional groups such as  $\text{COOH}$ ,  $\text{OH}$ , and  $-\text{O}-$  located at the edges of SWCNTs binding to the anatase or rutile  $\text{TiO}_2$  substrates. The binding regions have been found to have a higher electrostatic density that provides a better electron transfer. However, experimental studies also show that pure SWCNTs are also used as electron transfer facilitators through  $\text{TiO}_2$  supports.<sup>36,38,50</sup> We predict that, at the physical adsorption binding distance, SWCNTs provide a higher electron transfer compared to noncovalently and interfacially bound  $\text{TiO}_2$ –SWCNT, leading to improved insight into nanocomposite photocatalytic enhancement mechanisms.

A better understanding on the orientation of titania nanostructures on SWCNTs has been shown by performing electrostatic potential calculations on  $\text{TiO}_2$ –SWCNT systems. This study is of importance, as numerous experimental researchers have studied the transport route of photogenerated electrons in semiconducting electrodes such as  $\text{TiO}_2$ .<sup>37</sup> Both armchair and zigzag SWCNTs were found to have an excess of electrostatic potential located at the opposite direction of the binding region. Further improvements in the photovoltaic performances of the DSSCs can be achieved by predicting better interfacial interaction between  $\text{TiO}_2$  and SWCNTs.

These results show the utility of density functional theory for examining SWCNT– $\text{TiO}_2$  interactions for understanding the growth mechanisms for future experimental investigations with this promising system for photovoltaic and photocatalytic applications. The effect of rotations, for larger nanostructures on the strength of the binding energy of substrate–adsorbate systems, has been demonstrated theoretically to be of importance. Extension of our work for experimentally examining functionalization in pure and functionalized CNT–titania systems is ongoing.

## ASSOCIATED CONTENT

### Supporting Information

Supercell parameters are given for (5,5) armchair SWCNT and (8,0) zigzag SWCNT. Details of the organic functionalization of SWCNT substrates are included. Additional calculation details are provided for molecular  $\text{TiO}_2$ , rutile  $\text{Ti}_2\text{O}_4$ , and anatase  $\text{Ti}_4\text{O}_8$ . The Supporting Information is available free of charge on the ACS Publications website at DOI: 10.1021/acs.jpcc.5b01406.

## AUTHOR INFORMATION

### Corresponding Author

\*E-mail: pcharpentier@eng.uwo.ca.

### Notes

The authors declare no competing financial interest.

## ACKNOWLEDGMENTS

W.A.H. acknowledges EPSRC support for the UKCP consortium, Grant No. EP/K013610/1. S.A. and P.A.C. also thank the Natural Sciences and Engineering Research Council of Canada (NSERC) for funding this research and SHARC-Net for providing the computing facilities to perform the simulations. K.P. acknowledges the Bolyai Grant of the Hungarian Academy of Sciences.

## REFERENCES

- (1) Iijima, S. Helical Microtubules of Graphitic Carbon. *Nature* **1991**, *354*, 56–58.
- (2) Fthenakis, Z. G.; Tomanek, D. Computational Study of the Thermal Conductivity in Defective Carbon Nanostructures. *Phys. Rev. B* **2012**, *86*, 125418-1–125418-5.
- (3) Dresselhaus, M. S.; Dresselhaus, G.; Saito, R. Physics of Carbon Nanotubes. *Carbon* **1995**, *33*, 883–891.
- (4) Odom, T. W.; Huang, J. L.; Kim, P.; Lieber, C. M. Atomic Structure and Electronic Properties of Single-Walled Carbon Nanotubes. *Nature* **1998**, *391*, 62–64.
- (5) Wildoer, J. W. G.; Venema, L. C.; Rinzler, A. G.; Smalley, R. E.; Dekker, C. Electronic Structure of Atomically Resolved Carbon Nanotubes. *Nature* **1998**, *391*, 59–62.
- (6) Evarestov, R. A.; Bandura, A. B.; Losev, M. V. Symmetry and Stability of Nanotubes Based on Titanium Dioxide. *Russ. J. Gen. Chem.* **2010**, *80*, 1152–1167.
- (7) Chelmecka, E.; Pasterny, K.; Kupka, T.; Stobinski, L. DFT Studies of COOH Tip-Functionalized Zigzag and Armchair Single Wall Carbon Nanotubes. *J. Mol. Model.* **2012**, *18*, 2241–2246.
- (8) Chelmecka, E.; Pasterny, K.; Kupka, T.; Stobinski, L. OH-Functionalized Open-Ended Armchair Single-Wall Carbon Nanotubes (Swcnt) Studied by Density Functional Theory. *J. Mol. Model.* **2012**, *18*, 1463–1472.
- (9) Barone, V.; Heyd, J.; Scuseria, G. E. Interaction of Atomic Hydrogen with Single-Walled Carbon Nanotubes: A Density Functional Theory Study. *J. Chem. Phys.* **2004**, *120*, 7169–7173.
- (10) Beheshtian, J.; Peyghan, A. A.; Bagheri, Z. Carbon Nanotube Functionalization with Carboxylic Derivatives: A DFT Study. *J. Mol. Model.* **2013**, *19*, 391–396.
- (11) Chelmecka, E.; Pasterny, K.; Kupka, T.; Stobinski, L. DFT Studies of OH-Functionalized Open-Ended Zigzag, Armchair, and Chiral Single Wall Carbon Nanotubes. *Phys. Status Solidi A* **2011**, *208*, 1774–1777.
- (12) Long, R. Electronic Structure of Semiconducting and Metallic Tubes in  $\text{TiO}_2$ /Carbon Nanotube Heterojunctions: Density Functional Theory Calculations. *J. Phys. Chem. Lett.* **2013**, *4*, 1340–1346.
- (13) Clemens, P.; Wei, X.; Wilson, B. L.; Thomas, R. L. Anatase Titanium Dioxide Coated Single Wall Carbon Nanotubes Manufactured by Sonochemical-Hydrothermal Technique. *Open J. Compos. Mater.* **2013**, *3*, 21–32.

- (14) Xie, Y.; Heo, S. H.; Yoo, S. H.; Ali, G.; Cho, S. O. Synthesis and Photocatalytic Activity of Anatase TiO<sub>2</sub> Nanoparticles-Coated Carbon Nanotubes. *Nanoscale Res. Lett.* **2010**, *5*, 603–607.
- (15) Pelaez, M.; Nolan, N. T.; Pillai, S. C.; Seery, M. K.; Falaras, P.; Kontos, A. G.; Dunlop, P. S. M.; Hamilton, J. W. J.; Byrne, J. A.; O'Shea, K.; et al. A Review on the Visible Light Active Titanium Dioxide Photocatalysts for Environmental Applications. *Appl. Catal., B* **2012**, *125*, 331–349.
- (16) Varghese, O. K.; Paulose, M.; Grimes, C. A. Long Vertically Aligned Titania Nanotubes on Transparent Conducting Oxide for Highly Efficient Solar Cells. *Nat. Nanotechnol.* **2009**, *4*, 592–597.
- (17) Vivero-Escoto, J. L.; Chiang, Y. D.; C-Wwu, K.; Yamauchi, Y. Recent Progress in Mesoporous Titania Materials: Adjusting Morphology for Innovative Applications. *Sci. Technol. Adv. Mater.* **2012**, *13*, 013003-1–013003-9.
- (18) Landmann, M.; Rauls, E.; Schmidt, W. G. The Electronic Structure and Optical Response of Rutile, Anatase and Brookite TiO<sub>2</sub>. *J. Phys.: Condens. Matter* **2012**, *24*, 195503-1–195503-6.
- (19) Amtout, A.; Leonelli, R. Optical-Properties of Rutile near Its Fundamental-Band Gap. *Phys. Rev. B* **1995**, *51*, 6842–6851.
- (20) Tang, H.; Levy, F.; Berger, H.; Schmid, P. E. Urbach Tail of Anatase TiO<sub>2</sub>. *Phys. Rev. B* **1995**, *52*, 7771–7774.
- (21) Ayissi, S.; Charpentier, P. A.; Farhangi, N.; Wood, J. A.; Palotas, K.; Hofer, W. A. Interaction of Titanium Oxide Nanostructures with Graphene and Functionalized Graphene Nanoribbons: A DFT Study. *J. Phys. Chem. C* **2013**, *117*, 25424–25432.
- (22) Farhangi, N.; Ayissi, S.; Charpentier, P. A. Fe Doped TiO<sub>2</sub>-Graphene Nanostructures: Synthesis, DFT Modeling and Photocatalysis. *Nanotechnology* **2014**, *25*, 305601-1–305601-11.
- (23) Lucky, R. A.; Sui, R. H.; Lo, J. M. H.; Charpentier, P. A. Effect of Solvent on the Crystal Growth of One-Dimensional ZrO<sub>2</sub>-TiO<sub>2</sub> Nanostructures. *Cryst. Growth Des.* **2010**, *10*, 1598–1604.
- (24) Sui, R. H.; Lo, J. M. H.; Charpentier, P. A. Infrared and Computational Studies on Interactions of Carbon Dioxide and Titania Nanoparticles with Acetate Groups. *J. Phys. Chem. C* **2009**, *113*, 21022–21028.
- (25) Perdew, J. P.; Chevary, J. A.; Vosko, S. H.; Jackson, K. A.; Pederson, M. R.; Singh, D. J.; Fiolhais, C. Atoms, Molecules, Solids, and Surfaces - Applications of the Generalized Gradient Approximation for Exchange and Correlation. *Phys. Rev. B* **1992**, *46*, 6671–6687.
- (26) Kresse, G.; Furthmüller, J. Efficiency of Ab-Initio Total Energy Calculations for Metals and Semiconductors Using a Plane-Wave Basis Set. *Comput. Mater. Sci.* **1996**, *6*, 15–50.
- (27) Kresse, G.; Furthmüller, J. Efficient Iterative Schemes for Ab Initio Total-Energy Calculations Using a Plane-Wave Basis Set. *Phys. Rev. B* **1996**, *54*, 11169–11186.
- (28) Tonner, R. Adsorption of Proline and Glycine on the TiO<sub>2</sub>(110) Surface: A Density Functional Theory Study. *ChemPhysChem* **2010**, *11*, 1053–1061.
- (29) Blochl, P. E. Projector Augmented-Wave Method. *Phys. Rev. B* **1994**, *50*, 17953–17979.
- (30) Kresse, G.; Joubert, D. From Ultrasoft Pseudopotentials to the Projector Augmented-Wave Method. *Phys. Rev. B* **1999**, *59*, 1758–1775.
- (31) Monkhorst, H. J.; Pack, J. D. Special Points for Brillouin-Zone Integrations. *Phys. Rev. B* **1976**, *13*, 5188–5192.
- (32) Dresselhaus, M. S.; Dresselhaus, G.; Saito, R. Carbon-Fibers Based on C-60 and Their Symmetry. *Phys. Rev. B* **1992**, *45*, 6234–6242.
- (33) Jishi, R. A.; Dresselhaus, M. S.; Dresselhaus, G. Symmetry Properties of Chiral Carbon Nanotubes. *Phys. Rev. B* **1993**, *47*, 16671–16674.
- (34) Sivek, J.; Leenaerts, O.; Partoens, B.; Peeters, F. Adsorption of Titanium and Titanium Dioxide on Graphene: N and P-Type Doping. arXiv:1301.3654 [cond-mat.mtrl-sci], 2013.
- (35) Labat, F.; Baranek, P.; Adamo, C. Structural and Electronic Properties of Selected Rutile and Anatase TiO<sub>2</sub> Surfaces: An Ab Initio Investigation. *J. Chem. Theory Comput.* **2008**, *4*, 341–352.
- (36) Nguyen, T. M.; Nguyen, C. K.; Vu, T. M. P.; Duong, Q. V.; Pham, T. L.; Nguyen, T. C. A Study on Carbon Nanotube Titanium Dioxide Hybrids: Experiment and Calculation. *Adv. Nat. Sci.: Nanosci. Nanotechnol.* **2014**, *5*, 045018-1–045018-6.
- (37) Chen, J. Z.; Li, B.; Zheng, J. F.; Zhao, J. H.; Zhu, Z. P. Role of Carbon Nanotubes in Dye-Sensitized TiO<sub>2</sub>-Based Solar Cells. *J. Phys. Chem. C* **2012**, *116*, 14848–14856.
- (38) Jang, S. R.; Vittal, R.; Kim, K. J. Incorporation of Functionalized Single-Wall Carbon Nanotubes in Dye-Sensitized TiO<sub>2</sub> Solar Cells. *Langmuir* **2004**, *20*, 9807–9810.
- (39) Liang, Y. T.; Vijayan, B. K.; Lyandres, O.; Gray, K. A.; Hersam, M. C. Effect of Dimensionality on the Photocatalytic Behavior of Carbon-Titania Nanosheet Composites: Charge Transfer at Nanomaterial Interfaces. *J. Phys. Chem. Lett.* **2012**, *3*, 1760–1765.
- (40) Niu, M.; Cheng, D. J.; Cao, D. P. Understanding the Mechanism of Photocatalysis Enhancements in the Graphene-Like Semiconductor Sheet/TiO<sub>2</sub> Composites. *J. Phys. Chem. C* **2014**, *118*, 5954–5960.
- (41) Savara, A. Standard States for Adsorption on Solid Surfaces: 2d Gases, Surface Liquids, and Langmuir Adsorbates. *J. Phys. Chem. C* **2013**, *117*, 15710–15715.
- (42) Mo, S. D.; Ching, W. Y. Electronic and Optical-Properties of 3 Phases of Titanium-Dioxide - Rutile, Anatase, and Brookite. *Phys. Rev. B* **1995**, *51*, 13023–13032.
- (43) Ostling, D.; Tomanek, D.; Rosen, A. Electronic Structure of Single-Wall, Multiwall, and Filled Carbon Nanotubes. *Phys. Rev. B* **1997**, *55*, 13980–13988.
- (44) Wang, C. C.; Zhou, G.; Liu, H. T.; Wu, J.; Qiu, Y.; Gu, B. L.; Duan, W. H. Chemical Functionalization of Carbon Nanotubes by Carboxyl Groups on Stone-Wales Defects: A Density Functional Theory Study. *J. Phys. Chem. B* **2006**, *110*, 10266–10271.
- (45) Sham, L. J.; Schlüter, M. Density-Functional Theory of the Energy-Gap. *Phys. Rev. Lett.* **1983**, *51*, 1888–1891.
- (46) Mori-Sánchez, P.; Cohen, A. J.; Yang, W. T. Localization and Delocalization Errors in Density Functional Theory and Implications for Band-Gap Prediction. *Phys. Rev. Lett.* **2008**, *100*, 146401-1–146401-4.
- (47) Charlier, J. C.; Ebbesen, T. W.; Lambin, P. Structural and Electronic Properties of Pentagon-Heptagon Pair Defects in Carbon Nanotubes. *Phys. Rev. B* **1996**, *53*, 11108–11113.
- (48) Geng, W.; Liu, H. X.; Yao, X. J. Enhanced Photocatalytic Properties of Titania-Graphene Nanocomposites: A Density Functional Theory Study. *Phys. Chem. Chem. Phys.* **2013**, *15*, 6025–6033.
- (49) Burgos, J. C.; Balbuena, P. B. Engineering Preferential Adsorption of Single-Walled Carbon Nanotubes on Functionalized St-Cut Surfaces of Quartz. *ACS Appl. Mater. Interfaces* **2014**, *6*, 12665–12673.
- (50) Yao, Y.; Li, G.; Ciston, S.; Lueptow, R. M.; Gray, K. A. Photoreactive TiO<sub>2</sub>/Carbon Nanotube Composites: Synthesis and Reactivity. *Environ. Sci. Technol.* **2008**, *42*, 4952–4957.